

RADIATION SCATTERING

PACS numbers: 87.64.Cc; 87.63.L–; 42.30.Wb
DOI: 10.1070/QE2015v045n06ABEH015665

Specific features of diffuse photon migration in highly scattering media with optical properties of biological tissues

S.G. Proskurin, A.Yu. Potlov, S.V. Frolov

Abstract. **Specific features of motion of photon density normalised maximum (PDNM) of pulsed radiation in highly scattering media with optical properties of biological tissues are described. A numerical simulation has confirmed that, when the object is a homogeneous cylinder, PDNM always moves to its geometric centre. In the presence of an absorbing inhomogeneity, PDNM moves towards the point symmetric to the geometric centre of the inhomogeneity with respect to the centre of the cylindrical object. In the presence of a scattering inhomogeneity, PDNM moves towards its geometric centre.**

Keywords: *highly scattering media, diffuse optical tomography, biological tissue, absorbing inhomogeneity, scattering inhomogeneity.*

1. Introduction

Optical radiation transmitted through a biological (biomedical) tissue contains information about the shape, sizes, location, and optical properties of its different parts [1, 2]. To apply this information, one must investigate the propagation of radiation through a specific biomedical object.

Photon migration in highly scattering media with optical properties of biological tissues can be modelled by the Monte-Carlo method (method of statistical tests) [3], applying the Kubelka–Munk method (many-flux model), or solving the radiative transfer equation in the diffusion approximation (RTE-DA) [4]. This equation describes fairly well the photon migration in large (from 5 to 15 cm in size), optically dense (with reduced scattering coefficient $\mu_s' = 0.5–2.0$ mm^{-1}) biomedical objects; to solve it, one does not need large computational resources [1, 4–7].

RTE-DA simulation can be performed using several different approaches. Photon density can be presented as a function of coordinate and time [time-resolved diffuse optical tomography (TR-DOT)] or as a function of coordinate and frequency [frequency-domain DOT (FD-DOT)].

In the former case, RTE-DA has the form

$$\frac{1}{c}\frac{\partial\phi(x,y,z,t)}{\partial t} - D(x,y,z)\nabla^2\phi(x,y,z,t) + \mu_a(x,y.z)\phi(x,y,z,t) = S(x,y,z,t),\ \forall(x,y.z)\in\Omega, \quad (1)$$

S.G. Proskurin, A.Yu. Potlov, S.V. Frolov Tambov State Technical University, ul. Sovetskaya 106, Tambov, 392000 Russia;
e-mail: spros@tamb.ru, zerner@yandex.ru

Received 29 August 2014
Kvantovaya Elektronika **45** (6) 540–546 (2015)
Translated by Yu.P. Sin'kov

where $c = c_0/v_{object}$, c_0 is the speed of light in the medium and vacuum; v_{object} is the relative refractive index of the modelled object Ω and its boundary $\partial\Omega$; $x, y,$ and z are the coordinates of all points of the finite modelled region, including the internal part of the modelled object Ω, its boundary $\partial\Omega$, radiation source q, and detectors at this boundary; $D(x,y,z) = \{3[\mu_a(x,y,z) + (1 - g(x,y,z))\mu_s(x,y,z)]\}$ is the diffusion coefficient at points with coordinates $x, y,$ and z; $\mu_a(x,y,z)$ and $\mu_s(x,y,z)$, respectively, the absorption and scattering coefficients at points with coordinates $x, y,$ and z; g is the anisotropy parameter (average cosine of the scattering angle); $\phi(x,y,z,t)$ is the photon density at point $r(x,y,z)$ with coordinates $x, y,$ and z at instant t; and $S(x,y,z,t)$ is the photon source function at point q [5, 7].

In the case of FD-DOT, one measures a decrease in the intensity and the phase shift of probe radiation, and RTE-DA takes the form

$$\frac{1}{c}i\omega\widehat{\phi}(x,y,z,\omega) - D(x,y,z)\nabla^2\widehat{\phi}(x,y,z,\omega) + \mu_a(x,y,z) \times\widehat{\phi}(x,y,z,\omega) = \widehat{S}(x,y,z,\omega),\ \forall(x,y,z)\in\Omega, \quad (2)$$

where ω is the amplitude modulation frequency for the radiation incident on the object and $\widehat{\phi}(x,y,z,\omega)$ and $\widehat{S}(x,y,z,\omega)$ are, respectively, the complex photon density and the complex photon source function [4, 7].

Equations (1) and (2) are related via Fourier transform; therefore, from the theoretical point of view, they are equally informative. Thus, the time-resolved information obtained at all instants is equivalent to the frequency-resolved information obtained for all frequencies [4, 5, 7]. However, in practice, TR-DOT yields a larger amount of information than FD-DOT. When femtosecond lasers were developed, measurements of the time-dependent scattering function of point in a (3–7)-ns window at multiple instants became more convenient than FD-DOT measurements with a multiple frequency in a frequency band $\sim 10^{13}$ Hz, which corresponds to a 100-fs pulse.

Experimental FD-DOT setups use amplitude modulation of cw radiation at several frequencies rather than an infinite frequency band [4, 8]. Theoretically, the spatial resolution of this system increases with an increase in the modulation frequency of the probe radiation, whereas the sensitivity decreases. At a modulation frequency above 1 GHz, it is practically impossible to record the phase difference at the input and output of a biological object; in addition, the probe depth is so small in this case that the levels of useful signal and noise become comparable [5].

In this context, we apply Eqn (1) in this study. The form of the source function $S(x,y,z,t)$ calls for individual consideration.

A solution to Eqn (1) for objects with very simple geometry (an infinite or semi-infinite homogeneous medium and an infinite homogeneous rectangular parallelepiped) was used in [1, 4–7]. For these objects, the radiation source is considered to be an infinitely short pulse: $S(x_0,y_0,z_0,t_0) = \delta(x_0,y_0,z_0,t_0)$, where δ is delta function. In homogeneous cases with very simple geometries, one does not need to solve numerically Eqn (1): the function $\phi(x,y,z,t)$ is found analytically using Green's function [5]:

$$\phi(x,y,z,t) = \frac{1}{[4\pi cD(t-t_0)]^{3/2}} \times \exp\left[-\frac{(x-x_0)^2-(y-y_0)^2-(z-z_0)^2}{4cD(t-t_0)} - \mu_a(x,y,z)c(t-t_0)\right].$$

Another analytical solution for an infinite homogeneous medium was reported in [8, 9]:

$$\phi(x,y,z,t) = \left(\frac{3}{4\pi t}\right)^{3/2} \exp\left[-\frac{r(x,y,z)}{4cDt} - \mu_a(x,y,z)ct\right].$$

This solution is based on the use of a source exponentially decaying in the beam propagation direction (in the case of a Gaussian pulse) [9, 10]. However, this approach was initially formulated for cw radiation decaying in a tissue and cannot be used for TR-DOT.

The photon migration in an infinite rectangular parallelepiped is simulated using a collimated beam incident on the object normally to its surface. In this case, a point virtual isotropic source is formed at depth $z_0 = 1/\mu_s'$ (average scattering length):

$$S(x,y,z,t) = \delta(x,y,z-x_0,y_0,z_0)\,\delta(t-t_0), \quad (3)$$

In further consideration, it is assumed to be the only photon source in the object [1, 4, 6]. Then the analytical solution to Eqn (1) takes the form

$$\phi(x,y,z,t) = \frac{1}{[4\pi cD(t-t_0)]^{3/2}} \times \exp\left[-\frac{p^2}{4cD(t-t_0)} - \mu_a(x,y,z)c(t-t_0)\right] \times \left\{\exp\left[\frac{-(z-z_0)^2}{4cD(t-t_0)}\right] - \exp\left[\frac{-(z+z_0)^2}{4cD(t-t_0)}\right]\right\},$$

where $p = \sqrt{(x-x_0)^2-(y-y_0)^2}$.

When simulating more complex objects (finite cylinders, spheres, cones) and inhomogeneous objects, it is expedient to use the numerical solution within RTE-DA instead of the analytical solution. In this case, it is proposed to use the photon source function at the initial instant t_0 in the form (3) on the object boundary at point q.

In this paper, we report the results of studying the laws of motion of photon density maximum in homogeneous and inhomogeneous highly scattering cylinders. To reduce the distortions related to interpolation of photon density distribution, we performed numerical simulation by the finite-element method; the distances between grid points were the same for all three coordinate axes.

2. Photon density normalised maximum

The distribution of migrating-photon density in a three-dimensional finite cylinder, the optical properties of which correspond to those of biological tissues containing scattering particles, was simulated within the RTE-DA model, which describes the energy balance in the medium. Here, RTE is partial differential equation (1). The photon flux at the boundary of the modelled object is described using the Robin boundary condition [5, 7]:

$$\phi(x,y,z,t) + 2D(x,y,z)F\frac{\partial\phi(x,y,z,t)}{\partial n(x,y,z)} = 0,$$

$$\forall x,y,z \in \partial\Omega, \quad x,y,z \notin q, \quad (4)$$

where $n(x,y,z)$ is the direction of the external normal to boundary $\partial\Omega$ at point with coordinates x,y,z;

$$F = \frac{2/(1-R_0) - 1 + |\cos Q_c|^3}{1 - |\cos Q_c|^2}$$

is the Fresnel reflection coefficient [9, 11];

$$R_0 = \frac{(v_{object}/v_{medium} - 1)^2}{(v_{object}/v_{medium} + 1)^2}, \quad Q = \arcsin\frac{v_{medium}}{v_{object}}$$

are coefficients; and v_{medium} is the relative refractive index of the object environment (for air, $v_{medium} = 1$).

Equation (1) with the boundary condition (4) was solved numerically according to the seven-point template. The initial approximation of function $\phi(x,y,z,t)$ at all grid points is generated with allowance for the photon-source position and the number of photons per pulse [10–12]. The iterative process was over when the specified calculation time expired.

After the calculations, to make the photon density normalised maximum (PDNM) clearly seen, function $\phi(x,y,z,t)$ is normalised with respect to the current point with maximum density $\phi_{max}(x,y,z,t)$ at specified instants:

$$\phi_{norm}(x,y,z,t) = \frac{\phi(x,y,z,t)}{\phi_{max}(x,y,z,t)}.$$

Then the following transformation is carried out:

$$\phi_{norm}(x,y,z,t) = \begin{vmatrix} 1, \phi_{norm}(x,y,z,t) \geqslant P, \\ \phi_{norm}(x,y,z,t), \text{otherwise}, \end{vmatrix}$$

where P is the empirically chosen minimum photon-density level for the normalised maximum, $0 < P \leqslant 1$.

3. Results and discussion

The above-described model was implemented in the form of specialised software [13] using the LabVIEW dataflow visual programming language and environment.

Based on the results of numerical simulation of homogeneous and inhomogeneous cylindrical objects, we chose the necessary cutoff level for PDNM ($P = 0.995$). Figure 1 shows the position of cylindrical inhomogeneity in a cylindrical object. It is found that, in any homogeneous case, independent of the absorption coefficient $\mu_a(x,y,z)$ and scattering coefficient $\mu_s(x,y,z)$, PDNM moves towards the geometric centre of this object; this behaviour is in agreement with the

results of previous experiments [14, 15]. The photon densities in the cross section at half height of a homogeneous cylinder (where the optical fibres of the radiation source and detectors are located) at different instants are presented in Fig. 2. Coefficients $\mu_a(x,y,z)$ and $\mu_s'(x,y,z)$ for $\forall\ (x,y,z) \in \Omega$ are 0.004 and 0.5 mm^{-1}, respectively. The cylinder diameter and height $d = 68$ mm are the same as in experiment [12, 14].

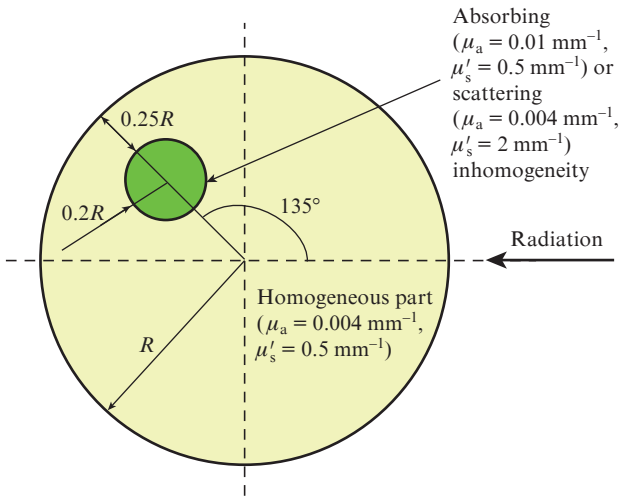

Figure 1. Cross section and optical properties of the cylindrical object under study with an incorporated cylindrical inhomogeneity.

When an object contains an absorbing inhomogeneity, the character of PDNM motion changes significantly. Figure 3 shows the photon distributions in the same cross section of a cylindrical object with a cylindrical absorbing inhomogeneity [$\mu_a(x,y,z) = 0.1$ mm^{-1}] at different instants. The inhomogeneity is located at an angle of 135° with respect to incident-beam axis at a depth of 0.25 of the object radius. This inhomogeneity is a cylinder with a diameter of 0.4 of the object radius; $R = d/2$ (Fig. 1). In the case of absorbing inhomogeneity, PDNM moves not to the centre of the object, as was suggested previously [14], but towards the point that is symmetric to the geometric centre of the inhomogeneity with respect to the cylindrical object axis.

The presence of a scattering inhomogeneity changes significantly the character of PDNM motion. Figure 4 shows the photon distribution in the cut of an inhomogeneous cylindrical object with a cylindrical scattering inhomogeneity, $\mu_s'(x,y,z) = 2$ mm^{-1}. In this case, PDNM moves towards the geometric centre of the inhomogeneity.

Let us denote the distance at which PDNM moves away from the geometric centre of the cylinder as L. Then, within the error related to the grid imposed on the object, one can state that $L \leqslant L^a_{crit}$, where L^a_{crit} is the distance from the centre of the modelled object to the point symmetric to the centre of this absorbing inhomogeneity with respect to the object axis. It is established that L depends on the optical and geometric properties of the modelled object. The dependence on its optical properties has the form

$$L = L^a_{crit}\left(1 - \frac{\mu_a^{hom}}{\mu_a^{inhom}}\right), \tag{5}$$

where μ_a^{hom} and μ_a^{inhom}, respectively, the average absorption coefficients of the homogeneous part of the object and the absorbing inhomogeneity. The scattering coefficient of the object with absorbing inhomogeneity only slightly affects L but determines the PDNM velocity.

The dependence of L on the geometric properties of the object is somewhat more complicated; it can be presented in the form

$$L = L^a_{crit}\left[\frac{\ln(S_{sum}S_{inhom}/S_{hom})}{\ln S_{sum}}\right], \tag{6}$$

where S_{hom} is the area of the homogeneous part of the object, S_{inhom} is the inhomogeneity area, and $S_{sum} = S_{hom} + S_{inhom}$ is the total area of the modelled object.

Having summed (5) and (6), we obtain the resulting dependence for calculating L in the case of single absorbing inhomogeneity:

$$L = \frac{L^a_{crit}}{2}\left[1 - \frac{\mu_a^{hom}}{\mu_a^{inhom}} + \frac{\ln(S_{sum}S_{inhom}/S_{hom})}{\ln S_{sum}}\right]. \tag{7}$$

When the object contains a single scattering inhomogeneity, the formula for L is similar. The difference is that, concerning the optical properties of the modelled object, the L value will be affected by the $\mu_s'^{hom}/\mu_s'^{inhom}$ ratio ($\mu_s'^{hom}$ is the average scattering coefficient of the homogeneous part of the object and $\mu_s'^{inhom}$ is the average reduced scattering coefficient of the inhomogeneity) rather than the $\mu_a^{hom}/\mu_a^{inhom}$ ratio. The absorption coefficient of the object with a scattering inhomogeneity does not affect the PDNM velocity and, therefore, is absent in the formula. The influence of the geometric properties of the object on L is retained in the form of (6).

Thus, the resulting formula for objects with a single scattering inhomogeneity can be written as

$$L = \frac{L^s_{crit}}{2}\left[1 - \frac{\mu_s'^{hom}}{\mu_s'^{inhom}} + \frac{\ln(S_{sum}S_{inhom}/S_{hom})}{\ln S_{sum}}\right], \tag{8}$$

where L^s_{crit} is the distance from the centre of the modelled object to the centre of scattering inhomogeneity. In the cases considered above (Figs 2–4), $L^s_{crit} = L^a_{crit}$ because of the identical geometry of inhomogeneity distribution.

An increase in the absorption coefficient of inhomogeneity and its size reduces the average (V^a_{avr}) and maximum (V^a_{max}) PDNM velocities. Table 1 contains velocities and minimum radii of curvature R^a_{cur} of PDNM trajectories for different coefficients μ_a of the absorbing inhomogeneity; $\mu_s' = 0.5$ mm^{-1} throughout the entire object. The PDNM motion velocities increase with an increase in the scattering coefficient of inhomogeneity and its size. Table 2 contains similar parameters for different scattering coefficients μ_s' of scattering inhomogeneity; $\mu_a = 0.004$ mm^{-1} throughout the object.

4. Conclusions

In the homogeneous case, independently of the values of absorption and scattering coefficients, the photon density maximum moves towards the geometric centre of the object. In the presence of an absorbing inhomogeneity, PDNM moves towards the point symmetric to the geometric centre of this inhomogeneity with respect to the centre of the cylindrical object. In the case of a scattering inhomogeneity, PDNM moves towards the centre of the latter. The distance at which PDNM moves away from the object geometric axis can be calculated using formulas (7) and (8).

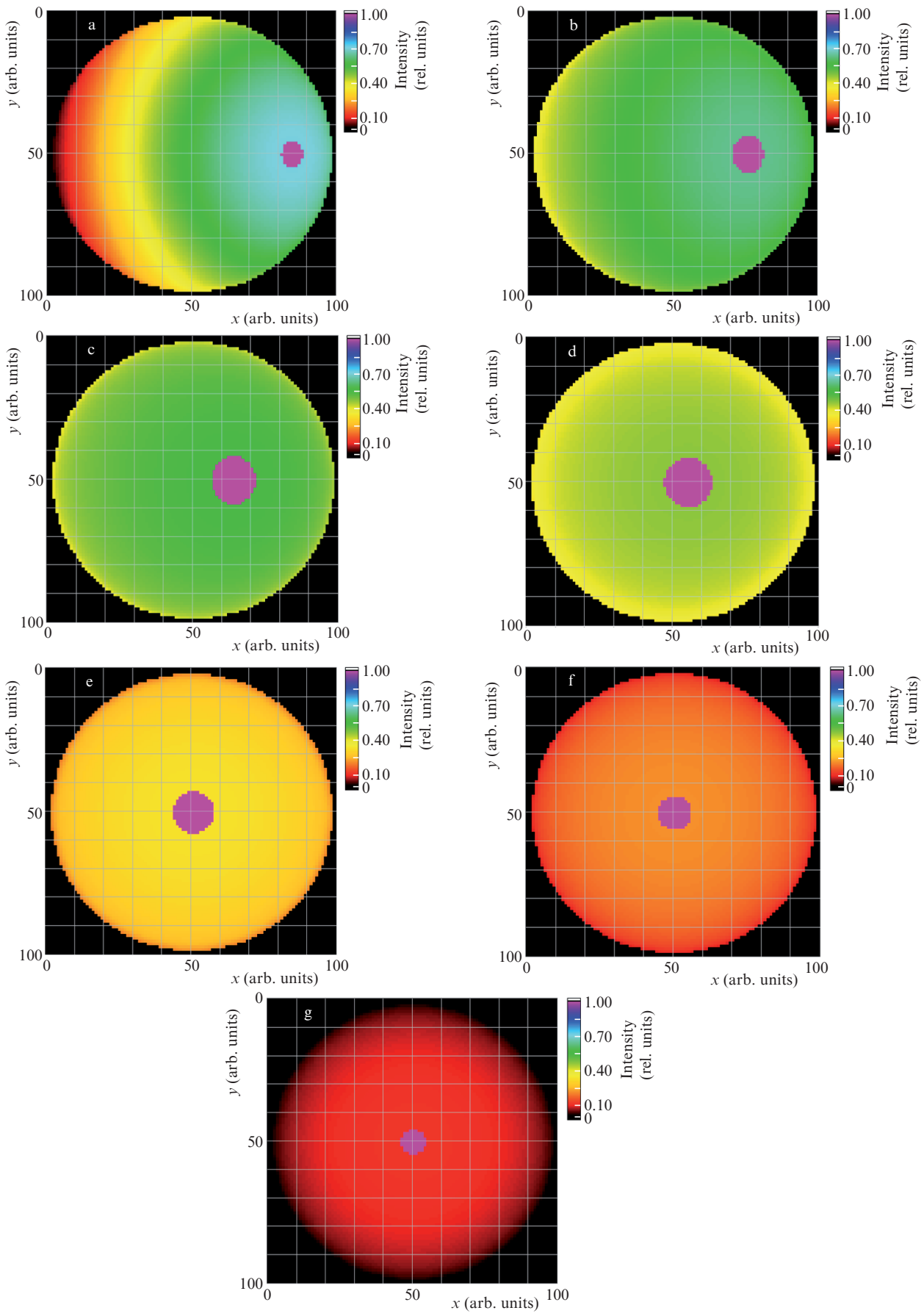

Figure 2. Photon distribution densities at half height of the homogeneous cylindrical object at instants of (a) 0.7, (b) 1.4, (c) 2.1, (d) 2.8, (e) 3.5, (f) 4.2, and (g) 4.9 ns. The spot shows the PDNM motion at a cutoff level of 0.5%.

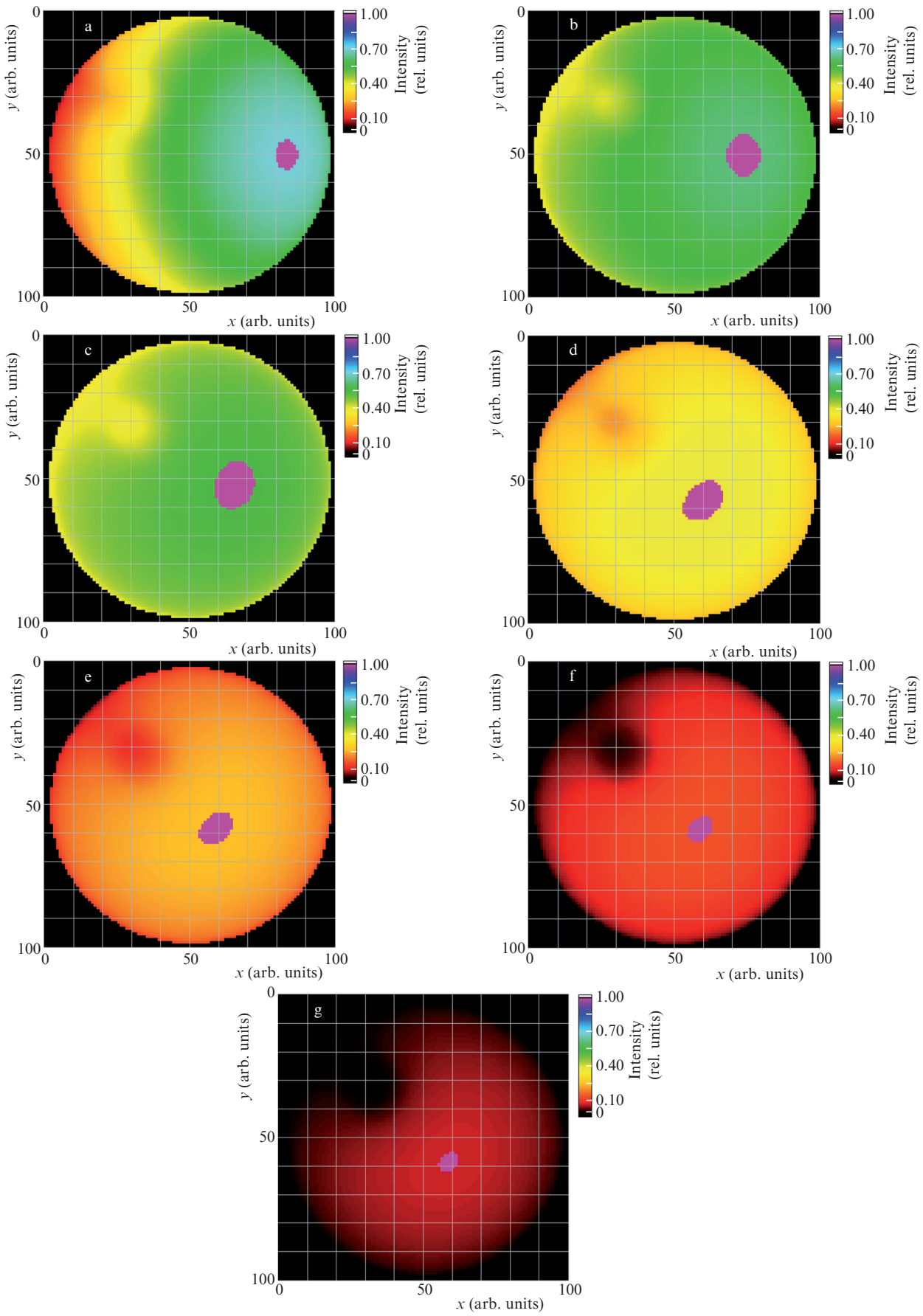

Figure 3. Photon distribution densities at half height of the inhomogeneous cylindrical object (absorbing cylindrical inhomogeneity) at instants of (a) 0.7, (b) 1.4, (c) 2.1, (d) 2.8, (e) 3.5, (f) 4.2, and (g) 4.9 ns. The spot indicates the PDNM location and shape at a cutoff level of 0.5%.

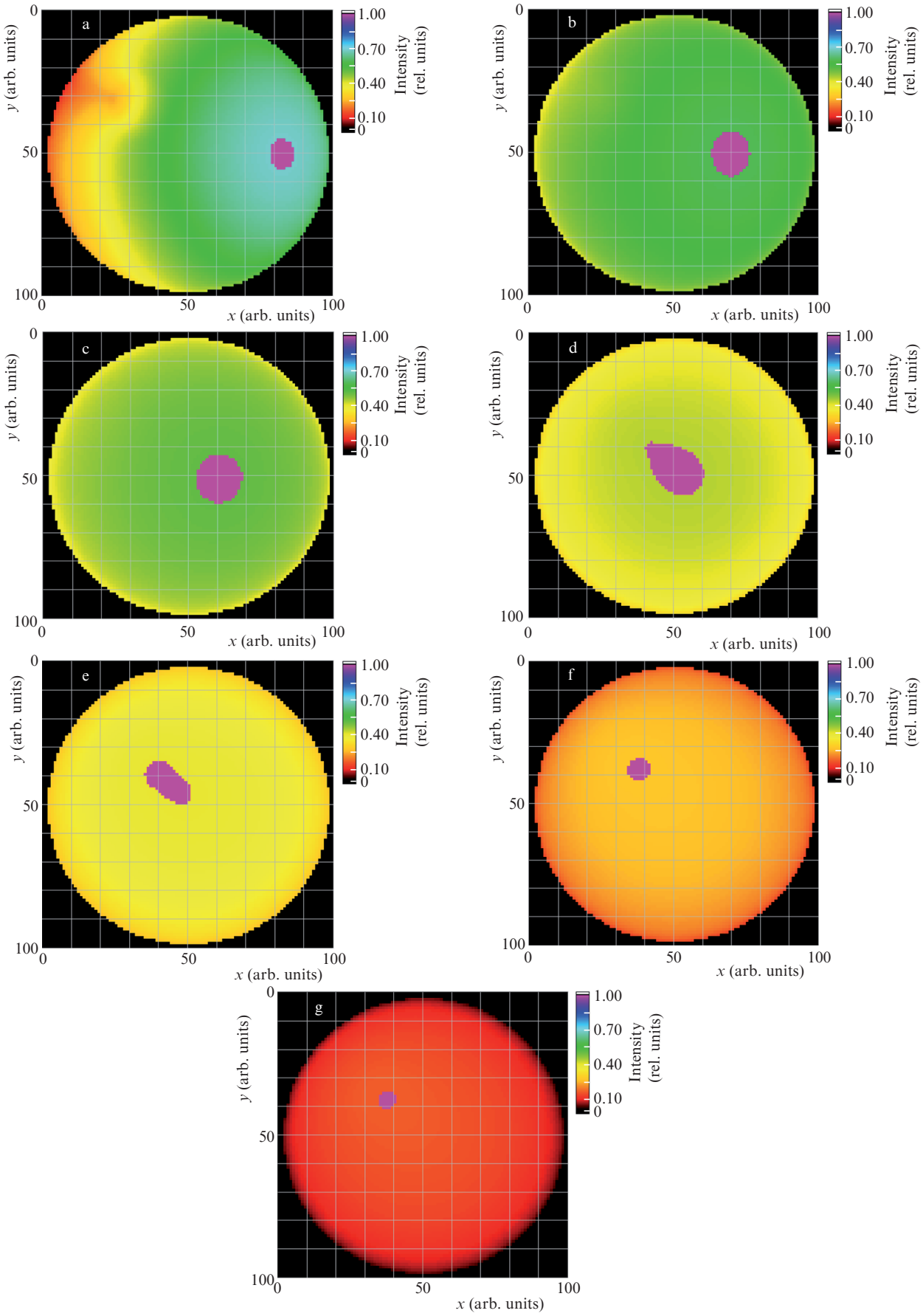

Figure 4. Photon distribution densities at half height of the inhomogeneous cylindrical object (scattering cylindrical inhomogeneity) at instants of (a) 0.9, (b) 1.8, (c) 2.7, (d) 3.6, (e) 4.5, (f) 5.4, and (g) 6.3 ns. The spot indicates the PDNM location and shape at a cutoff level of 0.5%.

Table 1. Average (V^{a}_{avr}) and maximum (V^{a}_{max}) velocities of PDNM motion and minimum radii of curvature R^{a}_{cur} of motion trajectories for different absorption coefficients μ_a of the absorbing inhomogeneity; μ'_s = 0.5 mm^{-1} throughout the entire object.

μ_a/mm^{-1}	V^{a}_{avr}/mm ns^{-1}	V^{a}_{max}/mm ns^{-1}	R^{a}_{cur}/mm
0.005	6.4	31.5	2.5
0.01	6.3	31.5	3.1
0.02	6.3	30.1	3.7
0.04	6.1	30.6	4.4
0.08	5.9	30.1	4.9
0.16	5.9	29.4	5.3
0.32	5.6	29.0	5.9
0.64	5.4	28.6	6.3

Table 2. Average (V^{s}_{avr}) and maximum (V^{s}_{max}) velocities of PDNM motion and minimum radii of curvature R^{s}_{cur} of motion trajectories for different absorption coefficients μ'_s of the absorbing inhomogeneity; μ_a = 0.004 mm^{-1} throughout the entire object.

μ'_s/mm^{-1}	V^{s}_{avr}/mm ns^{-1}	V^{s}_{max}/mm ns^{-1}	R^{s}_{cur}/mm
1	4.7	26.7	8.6
2	5.3	34.2	9.9
4	5.7	38.7	11.4
8	6.1	41.5	12.9
16	6.4	46.7	13.8
32	6.7	51.2	15.2
64	7.1	56.4	16.3

The rate of decrease in the total number of photons in cases with absorbing inhomogeneities (Fig. 3) is 10%–40% higher than in cases with scattering inhomogeneities (Fig. 4). The above-described model shows that in all cases the photon density maximum moves towards a point within the object and never passes through it, as was believed previously [3]. In addition, the model allows one to estimate the influence of the position and optical properties of inhomogeneities on the time-dependent scattering function of point and on the recorded photon leakage at object boundary $\partial\Omega$.

Acknowledgements. This work was supported by the Scholarship of the President of the Russian Federation, 2013 (Grant No.SP-4213.2013.4), and State Contract for Development of Medical Technologies No. 1.10.07.2014.

References

1. Patterson M., Chance B., Wilson B. *Appl. Opt*., **28**, 2331 (1989).
2. Zimnyakov D.A., Tuchin V.V. *Kvantovaya Elektron*., **32** (10), 849 (2002) [*Quantum Electron*., **32** (10), 849 (2002)].
3. Wang L.V., Jacques S.L. *Comp. Meth. Progr. Biomed*., **61**, 163 (2000).
4. Schmidt F.E. *Ph. D. Thesis* (Univ. College London, 1999).
5. Arridge S., Cope M., Delpy D. *Phys. Med. Biol*., **37**, 1531 (1992).
6. Proskurin S.G., Yamada Y., Takahashi Y. *Opt. Rev*., **2** (4), 292 (1995).
7. Schweiger M., Arridge S. *J. Biomed. Opt*., **19** (4), 040801 (2014).
8. Chen J. *Ph. D. Thesis* (Univ. College London, 2012).
9. Durian D., Rudnick J.J. *Opt. Soc. Am. A*, **16**, 4 (1999).
10. Durduran T., Choe R., et al. *Rep. Progr. Phys*., **73**, 076701 (2010).
11. Tret'yakov E.V., Shuvalov V.V., Shutov I.V. *Kvantovaya Elektron*., **31** (11), 1095 (2001) [*Quantum Electron*., **31** (11), 1095 (2001)].
12. Proskurin S.G., Potlov A.Y. *Photon. Las. Med*., **2** (2), 139 (2013).
13. Proskurin S.G., Frolov S.V., Potlov A.Yu. *Certificate of Governmental Registration of Computer Program in FIPS*, No. 2014613130 (2013).
14. Proskurin S.G. *Kvantovaya Elektron*., **41** (5), 402 (2011) [*Quantum Electron*., **41** (5), 402 (2011)].
15. Proskurin S.G., Potlov A.Yu., Frolov S.V. *Med. Tekh. (Moscow)*, **6** (276), 1 (2012).